Anal. Bioanal. Electrochem., Vol. 14, No. 11, 2022, 998-1010

Analytical & Bioanalytical Electrochemistry

2022 by CEE
www.abechem.com

Full Paper

Morphology and Oxidation State Dependent Glucose Sensing Properties of Cu-Oxide Nanocrystals

Carla Jacobs and Elizabeth Erasmus*

Department of Chemistry, University of the Free State, Bloemfontein 9300, South Africa

*Corresponding Author, Tel.: +27-514019656

E-Mail: erasmuse@ufs.ac.za

Received: 3 August 2022 / Received in revised form: 16 November 2022 / Accepted: 22 November 2022 / Published online: 30 November 2022

Abstract- Several morphologically different Cu-oxide nanocrystals (cube, exposing only the (100) facets; elongated octahedron, exposing only the (111) facets; normal octahedron, exposing only the (111) facets; rounded octahedron, exposing only the (111) facets; truncated edge cube, exposing the (100), (110), and (111) facets) have been prepared. Mixed oxidation state facets were obtained, with the X-ray Photoelectron Spectroscopy revealing that both Cu^{I} and Cu^{II} are present in the samples. The % Cu^{I} and Cu^{II} vary for the different morphologies. Morphologies exposing the (111) facet showed the highest % Cu^{I} present, with the morphologies exposing the (100) facet showing the least amount of Cu^{I}. The glassy carbon electrode's surface was modified with these Cu-oxide nanocrystals and their sensing performance for glucose detection was investigated. The limits of detection (LOD) observed for all the Cu-oxide nanocrystal electrodes were < 2 μM. Electrodes modified with Cu-oxide nanocrystals exposing the (111) facets and having more Cu^{I} present in the sample resulted in better glucose detection limits.

Keywords- Cu-oxide; Nanocrystals; Non-enzymatic glucose sensor; XPS; Oxidation state

1. INTRODUCTION

The detection of glucose is very important in many sectors of human activities. The detection and monitoring of glucose is employed in the clinical diagnosis of diabetes mellitus

[1], the measuring of the sugar content of a variety of foods and drinks [2,3], and even the measuring of glucose in a bioreactor or cell culture [4].

Diabetes mellitus is a major health problem worldwide, per year over one million deaths can be attributed to diabetes, resulting in diabetes being the 9th leading cause of mortality [5]. Due to diabetes being such a cause of concern, the need for low-cost sensors with a high reliability and sensitivity, good selectivity and fast response for detection and monitoring of glucose levels, has significantly increased [6].

Glucose-sensors are mainly categorised in two groups, namely non-enzymatic and enzymatic detectors. The most used sensors are enzyme-based and focuses on using glucose oxidase due to their excellent sensitivity and selectivity [7]. Although, due to the insufficient stability of the sensor as a consequence of the intrinsic sensitivity of the enzyme to temperature and pH, their reliability is brought in to question [8]. This drives the need for suitable non-enzymatic sensors which provide the same level of accuracy and sensitivity as their enzymatic counterparts.

Cu_2O based-materials have exhibited great potential for glucose oxidation [9], as it is a semi-conductor that is non-toxic, and possesses good chemical stability, electrochemical activity, and low-cost synthetic process. Using bulk sized Cu_2O, glucose detection is measured in an excess glucose solution which is not suitable for home-type or rapid testing. However, nanosized Cu_2O have shown great potential towards non-enzymatic glucose detection [10–12], owing to their good catalytic activity, chemical stability, biological compatibility and controllable size [13]. A variety of interesting morphologies of different copper nanoparticles and nanocomposites such: ultra-long Cu micro-dendrites [14], flower-like CuO nanostructures [15], 3D foam CuO [16], Cu_2O/RGO [17], GC/NiCu [18], Cu/Ni alloy [19], Cu- and CuO modified glass [20,21], have been successfully employed for non-enzymatic glucose sensing. Seeing as the properties of nanoparticles depend on the shape of the particle, controlling the morphology and also the exposed facets could enhance the performance of Cu_2O glucose sensors.

With the developments in colloidal synthesis, Cu_2O nanocrystals with a definite morphology exposing specific facets can be prepared [22,23]. Limited reports are available on the use of Cu_2O nanocrystals as non-enzymatic glucose sensors [24–26].

To expand the knowledge and potential use of Cu_2O nanocrystals as non-enzymatic glucose sensors, we have prepared cubic, elongated octahedron, normal octahedron, rounded octahedron, and truncated edge cubic Cu_2O nanocrystals. Cyclic voltammetry (CV) and chronoamperometry (CA) were conducted on Cu_2O nanocrystal modified glassy carbon electrodes to determine the detection capability for glucose. The glucose detecting performance of the Cu-oxide modified electrodes was related to the morphology and oxidation states of the Cu in the nanocrystals.

2. EXPERIMENTAL SECTION

Reagent grade chemicals (Sigma-Aldrich) and double distilled water were used.

2.1. Preparation of Cu_2O nanocrystals

$CuCl_2{\cdot}2H_2O$ (~1.71 g, 10 mmol) was dissolved in distilled water (1 L). Different ratios of polyvinylpyrrolidone (PVP, MW = 10 000 g/mol) were added to the to $CuCl_2{\cdot}H_2O$ solution to synthesize different morphologies of Cu_2O nanocrystals. A summary of the reagents and quantities added for the different nanoparticles are tabulated in Table . NaOH (2 M, 0.1 L) was added dropwise to the stirring Cu/PVP solution. The reaction was stirred for 30 minutes before adding ascorbic acid (0.6 M, 0.1 L) dropwise. The stirring continued for 3 h at a temperature of 55°C. The nanoparticles were collected via centrifugation (10 000 rpm at 15°C), followed by washing three times with distilled water and twice with ethanol. These particles were subsequently dried at 60°C overnight in a vacuum oven.

Table 1. Summary of reagents added to the different Cu_2O syntheses

Nanoparticle number	$CuCl_2{\cdot}2H_2O$ (g)	PVP (g)	PVP : $CuCl_2{\cdot}2H_2O$ Ratio
1	1.715	0	0
2	1.706	8.521	5
3	1.705	25.573	15
4	1.709	51.143	30
5*	2.284	0	0

*For NC **5**, the same procedure to prepare **1** was used, however the ascorbic acid concentration was 0.85M.

2.2. Characterization

A JEOL-JSM7800 Field Emission Scanning Electron Microscope was used to capture the SEM images at beam energies in the range of 5 keV. X-ray Photoelectron Spectroscopy (XPS) were measured on a PHI 5000 Versaprobe system with a monochromatic AlK X-ray source. The parameters used are similar to previously published methods [39–41].

2.3. Electrochemical measurements

The Cu-oxide solution is prepared by adding the appropriate nanoparticle (20 mg) in MeOH (0.5 mL), followed by sonication. The Cu-oxide solution (20 µL) is drop-coated onto the polished glassy carbon electrode surface (surface area = 0.0707 cm^2). After drying, Nafion (20 µL) was dropped over the modified surface followed by drying in air. The as-prepared modified glassy carbon electrodes (**1-5**/GC) was utilized for the working electrode while a Pt-wire acted as the counter electrode and a Ag^+/AgCl electrode was employed to be the reference electrode. The cyclic voltammetry and amperometric experiments were performed in 15 mL of 0.1 M NaOH aqueous solution in the presence of no glucose, 0.01 M glucose and 0.1 M glucose. The

amperometric study was conducted by successive addition of 50 μL of a 0.1 M glucose solution into the stirring NaOH solution having a set potential of 0.55 V. These experiments were conducted at room temperature.

3. RESULTS AND DISCUSSION

3.1. Synthesis of Cu-oxide nanocrystals

Different Cu-oxide nanocrystals (cube, **1**, elongated octahedron, **2**, normal octahedron, **3**, rounded octahedron, **4**, the truncated edge cube, **5**) were synthesized via a colloidal synthesis procedure (see Figure 1 the preparation), in the presence of polyvinylpyrrolidone (PVP). PVP exhibits selective surface stabilization on the (111) surfaces of Cu-oxide and by altering the quantity of PVP added to the mixture, the surface area ratio of the (111) and (100) facets can be controlled [27]. This resulted in the shape evolution of the copper oxide nanocrystals.

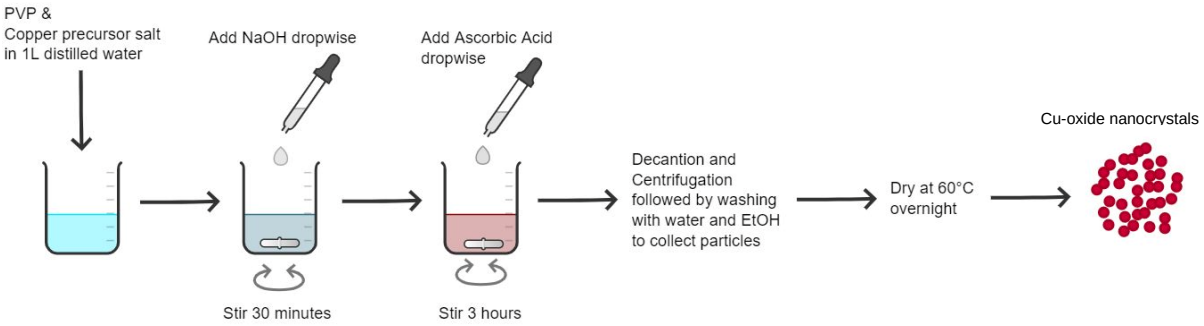

Figure 1. Schematic illustrating the experimental procedure followed during the preparation of copper oxide nanoparticles with defined morphology.

The morphologies of the copper oxide structures were explored by Scanning Electron Microscopy (SEM), see the images in Figure 2A-E. The cubic Cu-oxide nanocrystals (see Figure 2A for **1**) formed in the absence of PVP, as it is the thermodynamically stable form of Cu-oxide [27]. The cube shape consists of six exposed (100) facets. As the ratio of PVP to $CuCl_2 \cdot H_2O$ is increased to 5:1, the ratio of the (111) facets to the (100) facets increase. This resulted in the evolution of the shape from cubed to an elongated octahedron (see Figure B for **2**). Increasing this ratio to 15:1 resulted in the formation of a normal aspect ratio octahedron (see Figure 2C for **3**). (The method used to assign **2** as elongated in comparison to **3**, is shown in Figure 2F). However, when the PVP to $CuCl_2 \cdot H_2O$ was 30:1, the planes, corners, and edges of the octahedron become rounded (see Figure 2D for **4**). This indicated the importance of adding the correct amount of PVP to produce the desired morphology.

When the reaction in the absence of PVP (similar to the preparation of **1**) was repeated but with a slightly higher concentration of ascorbic acid (the reducing agent), a cubic structure was

again obtained but the sharp edges and corners were truncated, causing a truncated edge cube exposing the (100), (110) and (111) facets (see Figure E for **5**).

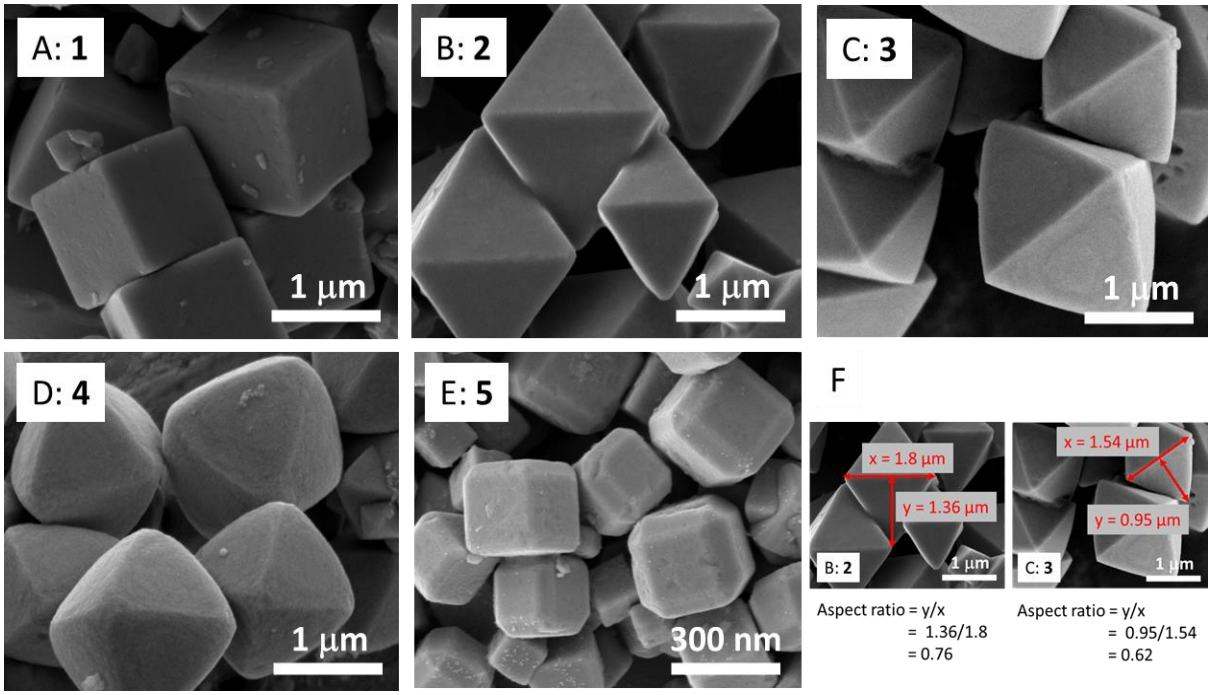

Figure 2. SEM images of the synthesized Cu_2O nanocrystals, illustrating the shape variation as a consequence of the PVP:$CuCl_2{\cdot}H_2O$ ratio: for (A) cube, **1**, the ratio = 0:1; (B) elongated octahedron, the ratio = 5:1; (C) normal octahedron, **3**, the ratio = 15:1; (D) rounded octahedron, **4**, the ratio = 30:1; (E) the truncated edge cube, **5**, the ratio = 0:1, however the ascorbic acid concentration was increased ca. 1.4 times; (F) Illustration of the method used to determine the aspect ratio of octahedrons **2** and **3**

X-ray photoelectron spectroscopy (XPS) was utilised to explore the copper's oxidation state present in **1-5**. As shown in Figure 3A (presenting the XPS of **1** as an example) the Cu $2p_{3/2}$ photoelectron area displayed a sharp well-defined photoelectron line with additional satellite structures. The Cu $2p_{3/2}$ envelope was deconvoluted using the simulated curve fitting parameter for Cu^{I} and Cu^{II} as proposed by Biesinger [28], The data extracted from the simulations of **1-5**, are summarized in Table 2. The Cu^{I} photoelectron line was located at *ca.* 932.7 eV, while the first peak of the Cu^{II} was found at *ca.* 934.3 eV. Using Biesinger's parameters the % amount of Cu^{I} and Cu^{II} could be determined. In all cases, the % Cu^{I} is in majority. The highest % Cu^{I} was found in the cubic structure (**1**, 84.2%), while the normal aspect ratio octahedron (**3**, 67.9%) displayed the least amount Cu^{I} present during the analysis. It is well known that Cu_2O tends to undergo irreversible redox disproportionation producing CuO [29]. Considering that the highest amount of Cu^{I} was found for **2-4**, exposing exclusively the (111) surface. This is consistent with the assumption that the Cu^{II} present on the (111)

surface is less stable towards redox disproportionation than the Cu^{II} on the (100) facet, resulting in a higher % Cu^{I} present.

Table 2. The binding energy as measured by XPS for the O 1s, and all the simulated peaks for the Cu $2p_{3/2}$ as well as the kinetic energy of the Cu LMM and Auger parameter, all measured in eV. The % Cu^{I} and Cu^{II} is also reported.

	O 1s (eV)	Cu^{I} $2p_{3/2}$ (eV)	Cu^{II} peak1 (eV)	Cu^{II} peak2 (eV)	Cu^{II} peak3 (eV)	Cu^{II} peak4 (eV)	Cu^{II} peak5 (eV)	Cu LMM (eV)	$Auger_{para}$ (eV)	% Cu^{I}	% Cu^{II}
1	532.0	932.8	934.7	936.1	942.1	943.3	944.3	916.4	1849.2	84.2	15.8
2	531.9	932.7	934.0	935.4	941.5	942.6	944.2	916.3	1849.0	68.2	31.8
3	531.0	932.5	934.1	935.5	941.5	942.6	944.1	916.3	1848.9	67.9	32.1
4	531.7	932.9	934.5	935.8	941.9	943.0	944.5	916.3	1849.2	73.5	26.5
5	531.7	932.4	934.9	936.3	942.4	943.5	945.6	916.9	1849.2	83.8	16.2

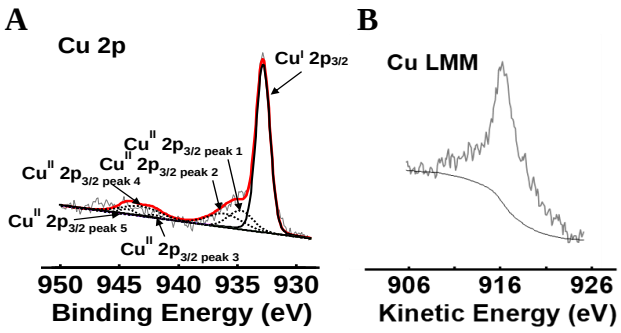

Figure 3. A: XPS spectra of the Cu $2p_{3/2}$ area of **1**; B: The Cu LMM Auger line of **1**

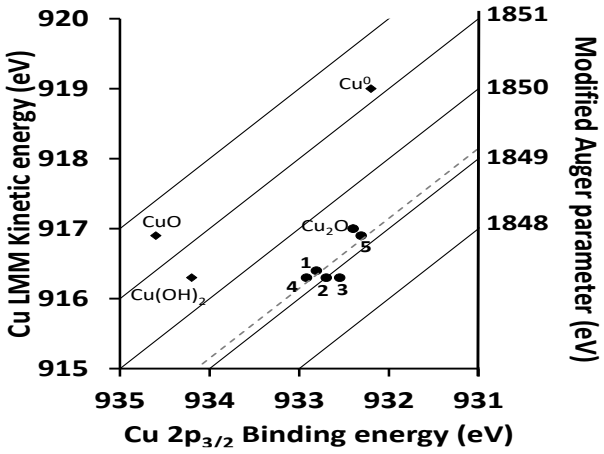

Figure 4. The Wagner plot for Cu indicating the data for **1**-**5** (●); Lines with a slope of -1, intersecting the y-axis (right hand side), designate α'. The data points of Cu^0, CuO, Cu_2O, and $Cu(OH)_2$ (♦) were obtained from Ref [32]

The kinetic energy (KE) of the Cu LMM Auger line (see Figure 3B, showing **1** as an example) was measured at *ca.* 916.4 eV and the modified Auger parameter, α', was calculated (α' = BE Cu $2p_{3/2\ main}$ + KE Cu_{LMM}) [30] to be *ca.* 1849.1 eV. From the Wagner plot, see Figure 4 (which is a graph with the BE of the Cu $2p_{3/2}$ on the x-axis, *vs* the kinetic energy of the Cu LMM plotted in the negative direction) [31], the trend line constructed for the data points of **1-5** and the reported values of Cu_2O, resulted in a line with a slope of *ca.* -1. Lines on the Wagner plot with a slope of -1 indicates species with the same oxidation state (further affirming that the majority of Cu present in the nanocrystals are Cu^I), and similar final state effects [30].

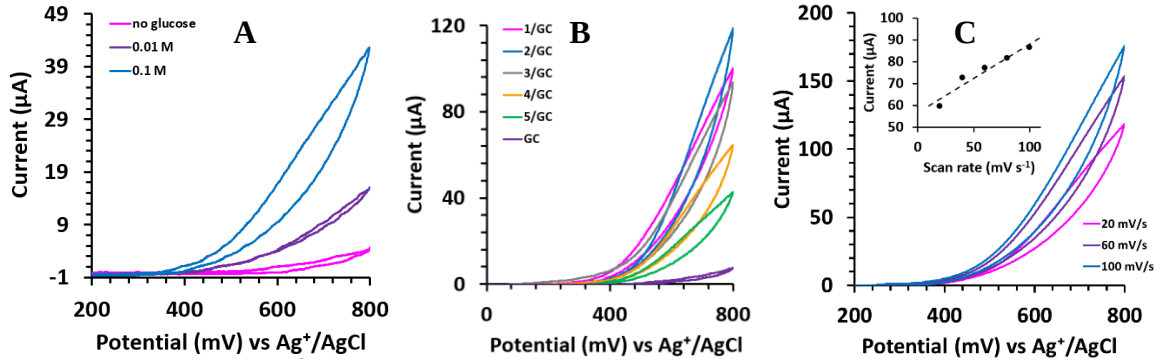

Figure 5. A: The CV curves of **5**/**GC** in 0.1 M aqueous NaOH containing either 0, 0.01, or 0.1 M glucose, measured at 20 mV s^{-1}; B: The CV curves of **1-5** /**GC** as well as unmodified glassy carbon in a mixture of 0.1 M NaOH and 0.1 M glucose, the CVs were measure at 20 mV s^{-1}. C: The CV curves of **2**/**GC** in a mixture of 0.1 M NaOH and 0.1 M glucose, measured at different scan rates of 20, 60 and 100 mV s^{-1}. Insert: The graph of the glucose oxidation current response (i_{pa}) *vs.* scan rate measured at $E_{p/2}$

The Cu-oxide nanocrystals were used to modify the glassy carbon electrode's surface (**1-5**/GC) and were explored for their potential use as non-enzymatic sensors for glucose detection. Their electrocatalytic activity for glucose oxidation was assessed by CV. From the CVs shown in Figure 5A of **5**/GC (shown as an example) in pure 0.1 M NaOH aqueous solution or a solution containing 0.01, and 0.1 M glucose (v = 20 mV s^{-1}), the current response escalates as the concentration of the glucose increase. The current response of the glucose-containing solutions contrasting the poor current response in the neat 0.1 M NaOH solution. Figure 5B shows the CV curves of **1-5**/GC as well as unmodified glassy carbon in a 0.1 M NaOH containing 0.1 M glucose, the CVs were acquired at 20 mV s^{-1}. No obvious detection of glucose was observed for the unmodified glassy carbon electrode, indicating that the Cu-oxide nanocrystals are responsible for the glucose oxidation/detection. **2**/GC, resulted in the highest oxidation current response (120 μA at 800 mV). As the scan rate increases the current response also increased (see Figure 5C, showing the CVs of **2**/GC as an example). The linear relationship

obtained by the Randles-Sevick graph (Figure C insert) indicative of electrochemical kinetics being controlled by adsorption of the glucose onto the electrode surface during the glucose oxidation [33].

The amperometric response curve of **1**/GC (shown as an example), indicating the consecutive addition of 50 μL of a 0.1 M glucose solution into 0.1 M NaOH, while stirring is shown in Figure 6. The applied potential was kept constant at 0.55 V during the amperometric sensing of glucose, seeing as at this potential, body fluid species will not interfere with the sensing [30].

A rapid increase in amperometric current is detected following the addition of the glucose (50 μL of 0.1 M glucose solution), with a steady state reached in seconds after addition of glucose. The graph constructed from the current response *vs* the added glucose concentration (Figure 6insert) displayed a linear relationship. The limit of detection (LOD) can be determined from data obtained from this relationship, LOD = $3s_x/m$, where s_x represents the standard deviation of the data set whereas m is the slope of the I *vs* [glucose] curve.

The normal physiological concentration of glucose in the human body is 4.4 – 6.1 mM [34], this value is higher than the LOD of all the electrodes (**1**-**5**/GC). The LOD (measured in μM) of **1**-**5**/GC as well as the sensitivity (measured in μA mM^{-1} cm^{-2}) are summarised in Table 2. The modified glassy carbon electrodes' (**1**-**5**/GC) performance is in line with the reported data of other Cu-based glucose sensing systems in literature (Table 3).

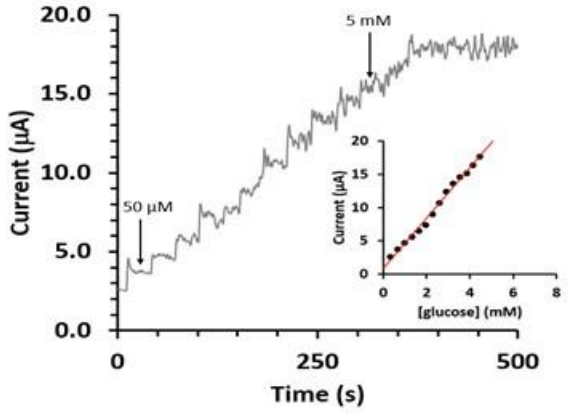

Figure 6. The amperometric response of the 1/GC electrode at 550 mV with the consecutive addition of 50 μL 0.1 M glucose to a 0.1 M NaOH solution every 30 s. Insert: The calibration curve of the current response versus the glucose concentration at the 1/GC electrode

The recyclability of the electrode was tested (using the same conditions, just washing the electrode surface with water. The graphs in Figure 7 shows that there is drop in current when moving from the first to the second run. Modified electrode surfaces **1/GC**, **2/GC** and **5/GC** showed the least amount of current drop, indication they are more stable.

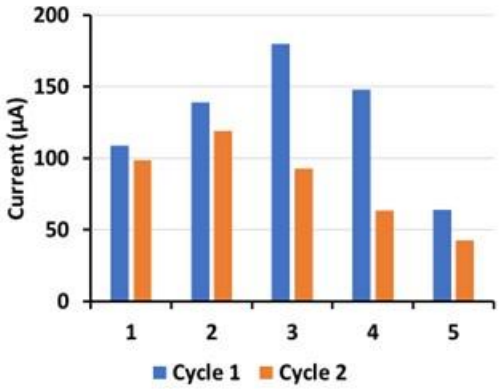

Figure 7. Graph showing the current measured (at a potential of 800 mV) for the first (blue bars) and second (orange bars) run of a 0.1 M glucose solution in 0.1 M NaOH at 20 mV s^{-1} for the modified glassy carbon electrode 1-5/GC

It has been reported that that the (111) facet is more polar than the (100) facet [24], resulting in faster electron transport across the (111) facet than the (100) facet. In correlation with this, higher electrochemical performance can be seen by the better glucose detection parameters (LOD and sensitivity) of the octahedron shaped samples of **2-3**/GC (exposing only the (111) facets) as compared the **1**/GC and **5**/GC exposing (100) facets. During the electrochemical sensing of glucose, the glucose gets oxidised at the Cu-oxide modified electrode.

Table 3. The LOD and sensitivity for glucose over **1-5**/GC electrodes; Also presenting comparative data from literature

	Applied potential	**Sensitivity ($\mu AmM^{-1}\ cm^{-2}$)**	**LOD (µM)**	
1/GC	0.55V[a]	41.30 (0.05)	1.46	Present work
2/GC	0.55V[a]	58.0 (0.1)	1.29	Present work
3/GC	0.55V[a]	37.9 (0.1)	1.06	Present work
4/GC	0.55V[a]	46.4 (0.2)	1.13	Present work
5/GC	0.55V[a]	17.9 (0.1)	1.57	Present work
octahedral Cu_2O–Nafion–GCE	0.65 V *vs* Hg/HgO	293.893	5.11	[24]
cubic Cu_2O–Nafion–GCE	0.65 V *vs* Hg/HgO	22.7	12.8	[24]
porous CuO microspheres	0.45 V *vs* SCE	349.6	0.5	[25]
3D graphene/Cu_2O	0.55	-	0.21	[25]
Au / Cu_2O nano-octahedrons	1.45	-	0.21	[35]
Cu_2O	0.4 V[a]	154	1.3	[36]
Cu-DA	0.5 V *vs.* SCE	223.17	20	[37]
Cu_2O/ Graphene	0.6 V[a]	285	3.3	[38]

[a] The potential was measured versus Ag^+/AgCl

This process involves the transfer of electrons between the glucose and the Cu-oxide modified electrodes. Thus, if the (111) facet of the Cu-oxide on the electrode results in more rapid electron transport from the electrode to the glucose, the response current would be higher, resulting in an electrode with better sensitivity towards the sensing of glucose.

Additionally, it was found that there is a relationship between the LOD of the modified glassy carbon electrodes (**1**-**5**/GC) and the amount of Cu^{II} present in the sample, see Figure 8. Lower Cu^{I} % and accordingly higher Cu^{II} % present (**3**/GC) resulted in a capability of detection of glucose at lower concentrations. This is in line with data reported for hydrogenation reactions of carbon dioxide over Cu_2O nano-cubes [29], where mixed oxidation state copper sites resulted in synergist effects with higher activity and stability

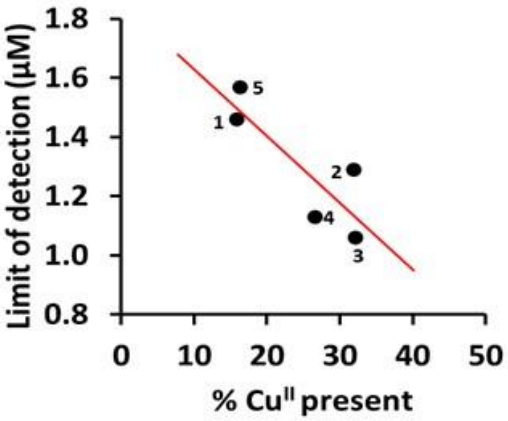

Figure 8. Graph showing the relationship between the limit of detection of the modified glassy carbon electrode **1**-**5**/GC and the % Cu^{II} present in the nanocrystals

Thus, for glucose detection it is not only the morphology exposing the (111) facets that is important but also the oxidation state of the Cu-oxide.

4. CONCLUSION

Cu-oxide nanocrystals were prepared by colloidal synthesis, the shape variation (exposed facets) was found to be a consequence of the PVP:$CuCl_2 \cdot H_2O$ ratio.

The non-enzymatic detection of glucose using the different Cu-oxide nanocrystal morphologies as electrode modifiers have been investigated. The Cu-oxide nanocrystals exposing the (111) facets showed in general a higher sensitivity with lower detection limits as compared to the nanocrystal exposing the (100) and/or (110) facets. Since the sensitivity increases on increasing % Cu^{II}, it can be concluded that the Cu^{II} favours the electrocatalytic effect. Additionally, the more Cu^{I} present in the sample, the better the glucose detection parameters were. Manipulation of the facet and oxidation state of Cu-oxide nanocrystals may result in superior selectivity in sensing and catalytic applications.

Supplementary information

Additional XPS spectra, CVs and amperometric response curves are provided in the Supporting Information.

Acknowledgements

The Sasol is acknowledged for financial support. The Central Research Fund of the University of the Free State, Bloemfontein, South Africa is also acknowledged for financial support.

Conflict of interest

The authors state that they have no conflicts of interest.

REFERENCES

[1] E. Renard, Ther. Allied Technol. 13 (2004) 78.
[2] D.P. Aykas, C. Ball, A. Menevseoglu, and L.E. Rodriguez-Saona, J. Appl. Sci. 10 (2020) 8774.
[3] J.P. Favier, D. Bicanic, P. Helander, and M. van Iersel, J. Biochem. Biophys. Methods. 34 (1997) 205.
[4] M. Tric, M. Lederle, L. Neuner, I. Dolgowjasow, P. Wiedemann, S. Wölfl, and T. Werner, Anal. Bioanal. Chem. 409 (2017) 5711.
[5] M.A.B. Khan, M.J. Hashim, J.K. King, R.D. Govender, H. Mustafa, and J. Al Kaabi, J. Epidemiol. Glob. Health 10 (2019) 107.
[6] F. Cao, and J. Gong, Anal. Chim. Acta 723 (2012) 39.
[7] S. Ferri, K. Kojima, and K. Sode, J. Diabetes Sci. Technol. 5 (2011) 1068.
[8] G. Liu, B. Zheng, Y. Jiang, Y. Cai, J. Du, H. Yuan, and D. Xiao, Talanta 101 (2012) 24.
[9] S.N.A.M. Yazid, I.M. Isa, and N. Hashim, Mater. Sci. Eng. C 68 (2016) 465.
[10] Z. Yu, C. Kong, J. Lv, B. Ma, X. Zhang, and Z. Yang, J. Solid State Electrochem. 24 (2020) 583.
[11] H. Yang, J. Bao, Y. Qi, J. Zhao, Y. Hu, W. Wu, X. Wu, D. Zhong, D. Huo, and C. Hou, Anal. Chim. Acta 1135 (2020) 12.
[12] F. Zhang, X. Xiao, J. Wang, S. Huang, H. Zhang, W. Zhang, X. Guo, D. Zhang, and M. Wang, Mater. Res. Express 6 (2019) 115049.
[13] E. Fazio, S. Spadaro, C. Corsaro, G. Neri, S.G. Leonardi, F. Neri, N. Lavanya, C. Sekar, N. Donato, and G. Neri, Sensors 21 (2021) 2494.
[14] D.J. Chen, Y.H. Lu, A.J. Wang, J.-J. Feng, T.T. Huo, and W.J. Dong, J. Solid State Electrochem. 16 (2012) 1313.
[15] N.G. Medeiros, V.C. Ribas, V. Lavayen, and J.A. Da Silva, J. Solid State Electrochem.

20 (2016) 2419.
[16] J. Hovancová, I. Šišoláková, R. Oriňaková, and A. Oriňak, J. Solid State Electrochem. 21 (2017) 2147.
[17] X. Yan, J. Yang, L. Ma, X. Tong, Y. Wang, G. Jin, and X.Y. Guo, J. Solid State Electrochem. 19 (2015) 3195.
[18] M. Jafarian, F. Forouzandeh, I. Danaee, F. Gobal, and M.G. Mahjani, J. Solid State Electrochem. 13 (2009) 1171.
[19] F. Wolfart, A. Maciel, N. Nagata, and M. Vidotti, J. Solid State Electrochem. 17 (2013) 1333.
[20] H.M. Yadav, and J.J. Lee, Solid State Electrochem. 23 (2019) 503.
[21] P. S, S. Berchmans, J. Solid State Electrochem. 16 (2012) 1527.
[22] E. Erasmus, J. Nanomater. 2020 (2020) 1.
[23] E. Erasmus, South African J. Chem. 75 (2021).
[24] L. Tang, J. Lv, C. Kong, Z. Yang, and J. Li, New J. Chem. 40 (2016) 6573.
[25] X. Liu, Y. Yang, R. Liu, Z. Shi, L. Ma, and M. Wei, J. Alloys Compd. 718 (2017) 304.
[26] Y. Jiang, T. Xia, L. Shen, J. Ma, H. Ma, T. Sun, F. Lv, and N. Zhu, ACS Catal. 11 (2021) 2949.
[27] D.-F. Zhang, H. Zhang, L. Guo, K. Zheng, X.-D. Han, and Z. Zhang, J. Mater. Chem. 19 (2009) 5220.
[28] M.C. Biesinger, Surf. Interface Anal. 49 (2017) 1325.
[29] L. Wan, Q. Zhou, X. Wang, T.E. Wood, L. Wang, P.N. Duchesne, J. Guo, X. Yan, M. Xia, Y.F. Li, A.A. Jelle, U. Ulmer, J. Jia, T. Li, W. Sun, and G.A. Ozin, Nat. Catal. 2 (2019) 889.
[30] C.D. Wagner, and A. Joshi, J. Electron Spectros. Relat. Phenomena. 47 (1988) 283.
[31] G. Moretti, J. Electron Spectros. Relat. Phenomena. 95 (1998) 95.
[32] M.C. Biesinger, Surf. Interface Anal. 49 (2017) 1325.
[33] L.C. Jiang, and W.D. Zhang, Biosens. Bioelectron. 25 (2010) 1402.
[34] C. Kong, L. Tang, X. Zhang, S. Sun, S. Yang, X. Song, and Z. Yang, J. Mater. Chem. A. 2 (2014) 7306.
[35] D. Chen, K. Xue, H. Liu, B. Yao, A. Sun, C. Liu, P. Zhang, and G. Cui, Nanomater. Nanotechnol. 11 (2021) 184798042110128.
[36] L. Zhang, Y. Ni, and H. Li, Microchim. Acta 171 (2010) 103.
[37] P. Viswanathan, J. Park, D.K. Kang, and J.D. Hong, Colloids Surfaces A Physicochem. Eng. Asp. 580 (2019) 123689.
[38] M. Liu, R. Liu, and W. Chen, Biosens. Bioelectron. 45 (2013) 206.
[39] E. Erasmus, J. Electron Spectros. Relat. Phenomena. 223 (2018) 84.
[40] E. Botha, M. Landman, P.H. van Rooyen, and E. Erasmus, Inorganica Chim. Acta 482 (2018) 514.

[41] A. Jansen van Rensburg, M. Landman, M.M. Conradie, E. Erasmus, and J. Conradie, Electrochim. Acta 246 (2017) 897.